Cation distribution and magnetic properties of LiMnZn ferrites

M. Arana[1], V. Galván[1], S. E. Jacobo[2], P. G. Bercoff[1]

[1]FaMAF, Universidad Nacional de Córdoba. IFEG-Conicet. Ciudad Universitaria. Córdoba. Argentina.
[2]LAFMACEL. Facultad de Ingeniería, UBA. Paseo Colón 850. Buenos Aires. Argentina.

Abstract

Spinel compounds $Li_{0.5x}Zn_{0.6-x}Mn_{0.4}Fe_{2+0.5x}O_4$ (x=0.0; 0.1; 0.2; 0.4) were produced by the self-combustion sol-gel method. The obtained powders were calcined at 1000ºC for 2 hours in Ar atmosphere. The structural and microstructural characteristics of the resulting samples were studied by magnetization measurements, Mössbauer spectroscopy and X-ray powder diffraction in combination with the Rietveld method. Based on magnetization results, a cation distribution model is proposed which is tested with Rietveld refinements and supported by Mössbauer results. The observed increase in saturation magnetization with Li content in the structure is explained by an unusual distribution of Zn^{2+} ions in octahedral sites.

Keywords: ceramics; oxide materials; crystal structure; magnetization; X-ray diffraction.

1. Introduction

It has been proved by many authors that the crystalline structure and physical properties of spinel ferrites are as strongly dependent on the preparation method and on the thermal treatment as they are on the doping element –if any [1].

Spinels crystallize in an fcc cubic structure containing tetrahedral (A) and octahedral (B) sites.

Though structurally simple, these materials can be compositionally complex. These compounds have the general formula $(Me_{1-\delta}Fe_{\delta})$ $[Me_{\delta}Fe_{2-\delta}]$, where Fe is in its trivalent state, "Me" represents a divalent metal element or any divalent combination of them, the parenthesis contain the cations in A sites and the square brackets the ones in B sites, and δ is the so-called degree of inversion (defined as the fraction of tetrahedral sites occupied by Fe^{3+} ions). Not all the available sites are occupied by cations and the proportion of tetrahedral to octahedral occupied sites is 1:2. Since ions in different sites are antiferromagnetically ordered, the resultant magnetism observed in ferrites is due to the unbalanced magnetizations of sublattices A and B [2].

The physical properties in general –and the magnetic behavior in particular– of a certain ferrite are determined by its microstructure. It is the distribution of a given element between both cation sites (which itself depends on cation size, valence, bond strength, temperature and pressure) that affects the physical properties. Mn-Zn ferrites have a mixed spinel structure. After the incorporation of new elements, the structural and magnetic environments of the two sites (A and B), can be quite different. Since the cationic distribution among the lattice sites is strongly dependent on the material's preparation [3-5], it is important to determine the cation sites occupancies as well as the structural parameters in order to control the material's performance.

A reliable method for such determination is the Rietveld analysis of X-ray powder diffraction patterns [6]. Different authors report the use of this analysis for obtaining information about the cationic distribution within the crystalline lattice [6-11].

Many studies have been developed on the magnetic, structural and morphologic properties in Mn-Zn ferrites mainly because of their novel applications in nanotechnology [9 - 15]. Different compounds, such as the spinel oxide $LiMn_{2-x}Zn_xO_4$ [10], ferrite $Li_xMn_{1+x}Fe_{2-2x}O_4$ [7] and other spinels of these elements [16-18] have been successfully characterized. In particular, De Fazio et al. reported interesting magnetic and electronic properties of the spinels $Li_{0.5x}Mn_{0.4}Zn_{0.6-x}Fe_{2+0.5x}O_4$ (x=0.0 to 0.4) [19, 20]. These authors found that Li for Zn

substitution –both non-magnetic ions– results in an enhancement in the magnetic properties and in an improvement of the micro-wave absorption characteristics.

In this work we correlate the magnetic and structural properties of $Li_{0.5x}Zn_{0.6-x}Mn_{0.4}Fe_{2+0.5x}O_4$ (x=0.0; 0.1; 0.2; 0.4) and determine the most probable cationic distribution in the spinel structure that agrees with both magnetic and structural experimental results.

2. Experimental

2.1. Samples preparation

Samples of composition $Li_{0.5x}Mn_{0.4}Zn_{0.6-x}Fe_{2+0.5x}O_4$ (x=0.0; 0.1; 0.2; 0.4) were prepared by the self-combustion of a citrate precursor, as explained elsewhere [19]. Once the sol-gel and posterior self-combustion was produced, the resulting residue was calcined at 1000°C for two hours in a static Ar atmosphere. The obtained samples were labeled 800, 801, 802 and 804, where the last digit indicates ten times the value of substitution, 0.5x in the stoichiometric formulation (see Table I).

Table I: Samples notation.

Sample	**x**	**Formulation**
800	0.0	$Mn_{0.4}Zn_{0.6}Fe_2O_4$
801	0.1	$Li_{0.05}Mn_{0.4}Zn_{0.5}Fe_{2.05}O_4$
802	0.2	$Li_{0.1}Mn_{0.4}Zn_{0.4}Fe_{2.1}O_4$
804	0.4	$Li_{0.2}Mn_{0.4}Zn_{0.2}Fe_{2.2}O_4$

2.2 Samples characterization

Structural characterization was performed by X-ray diffraction with a Philips PW3040/60 diffractometer, with Si monochromator, Cu-Kα incident radiation, at 40 kV and 30 mA, step scan of 0.2º/min and step size of 0.02º in 2θ. The different observed phases were refined with the Rietveld method, as implemented in the DiffracPlus TOPAS® commercial software..

^{57}Fe Mössbauer absorption spectra were recorded in transmission geometry at room temperature using a multichannel analyzer with a drive-in constant acceleration mode. A $^{57}Co(Rh)$ source with initial activity of 20mCi was used. The spectrometer was periodically calibrated using a natural iron foil as a standard. Powder samples (40 mg) were measured in a round acrylic sample holder of 20 mm diameter. The measured isomer shifts (IS); are referred to as α-Fe. The Normos/Site Program was used for fitting the measured spectra.

Magnetic properties were measured at room temperature with a vibrating sample magnetometer Lake Shore 7300 with a maximum applied field of 15 kOe. Magnetization as a function of temperature was measured for selected samples in a Quantum Design SQUID from 4 K to room temperature, with an applied field of 100 Oe.

2.3. XRD Rietveld refinements

The Rietveld refinement method uses a least squares approach to refine a theoretical X-ray diffraction spectrum until it matches the measured profile [21]. The model for the calculated profile includes structural (spatial groups, atoms in the asymmetric units, thermal factors, etc.), microstructural (concentration, crystal size, micro deformations) and instrumental (full width at half maximum, width of slits, size of the sample, depth of X-ray penetration, background, etc.) factors.

In the refinements performed in this work, the background was fitted using a sixth degree polynomial function and the parameters related to thermal fluctuations were not refined, since their influence is negligible compared to the uncertainties introduced by the refinement of

occupancy factors. The values for these thermal parameters were taken from the Inorganic Crystal Structure Database (ICSD) indexed files corresponding to each phase: ICSD #28514 for MnZn ferrite, #26170 for ZnO and # 24698 for FeO.

A TCHZ pseudo-Voigt profile was used to describe the peak shape. This function accounts separately for the contribution due to the particle size, the strain broadening and the experimental contribution (a detailed mathematical description of the Rietveld method can be found in ref. [21]). In order to account for the instrumental contribution, a standard reference material of silicon powder (SPI® SRM 640c) was measured.

2.3.1. Quality of fit

In order to provide figures of merit for the performance of the Rietveld method at the different refinement stages, indexes known as *R-factors* are usually used. The criteria used to determine the quality of the fit indicate the user the evolution of the refinement and help to decide if the proposed model is adequate. However, just a single parameter is not enough to evaluate the refinement [22], so it is important to have several indicators for each iteration. Different parameters appear in the literature to evaluate the quality of the fit [21]. In this work, the parameters called *weighted pattern* (R_{wp}), *goodness of fit* (*GoF*) and *expected factor* (R_{exp}) are used. These parameters are defined as:

$$R_{wp} = \sqrt{\frac{\sum w_n \left(Y_{o,n} - Y_{c,n}\right)^2}{\sum w_n \left(Y_{o,n} - Bkg_n\right)^2}},$$

$$GoF = \sqrt{\frac{\sum w_n \left(Y_{o,n} - Y_{c,n}\right)^2}{N - P}}$$

and

$$R_{\exp} = \frac{R_{wp}}{GoF}$$

where $Y_{o,n}$ and $Y_{c,n}$ are, respectively, the observed and calculated data at point *n;* Bkg_n, is the background at data point n*; N* is the number of data points; *P* is the number of parameters and w_n the weighting factor given to data point *n.* In counting statistics, this last factor is given by $w_n=1/\sigma(Y_{o,n})^2$, where $\sigma(Y_{o,n})$ is the error in $Y_{o,n}$.

Both R_{wp} and *GoF* are good global indicators of the refinement process, since the numerators of these factors contain the residual function which is being minimized. A rather good refinement is represented by low values of these parameters: R_{wp} around 0.10 for XRD in a conventional diffractometer, and *GoF* around 1 [23].

3. Results and discussion

Figure 1 shows the XRD patterns acquired for all the samples. Reflections of the (311), (440) and (220) planes confirm the formation of the MnZn ferrite with a well-defined spinel structure and some secondary phases which are indexed as ZnO and FeO. It is remarkable that sample 804 (with x=0.4) is single-phase.

Figure 2 shows the first quadrant of all the samples' hysteresis loops, all of which saturate at fields below 15 kOe. Li doping considerably modifies saturation magnetization M_s since its value increases from 63.0 emu/g for x=0.0 to 101.5 emu/g for x=0.4. The inset of Figure 2 shows the M_s values as a function of Li content, x. It is thought that the inclusion of Li^+ and extra Fe^{3+} in the lattice promotes a cation arrangement between tetrahedral and octahedral sites, increasing M_s to the rather high observed values. Since magnetization is given in emu/g, the M_s values for samples with secondary phases should be corrected. This is possible to do after refining the X-ray diffraction patterns, when the different phase's concentration are determined.

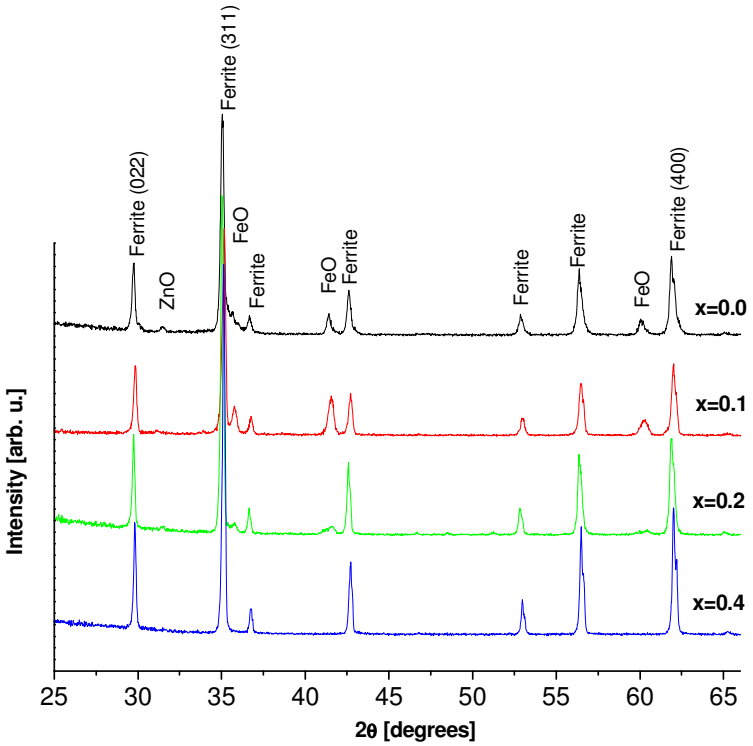

Figure 1: X-ray diffraction patterns of samples $Li_{0.5x}Zn_{0.6-x}Mn_{0.4}Fe_{2+0.5x}O_4$ (x=0.0; 0.1; 0.2; 0.4).

Coercivity is low in every case, with values around and below 100 Oe. A soft magnetic behavior has already been reported for MnZn ferrites [23] and is also expected here.

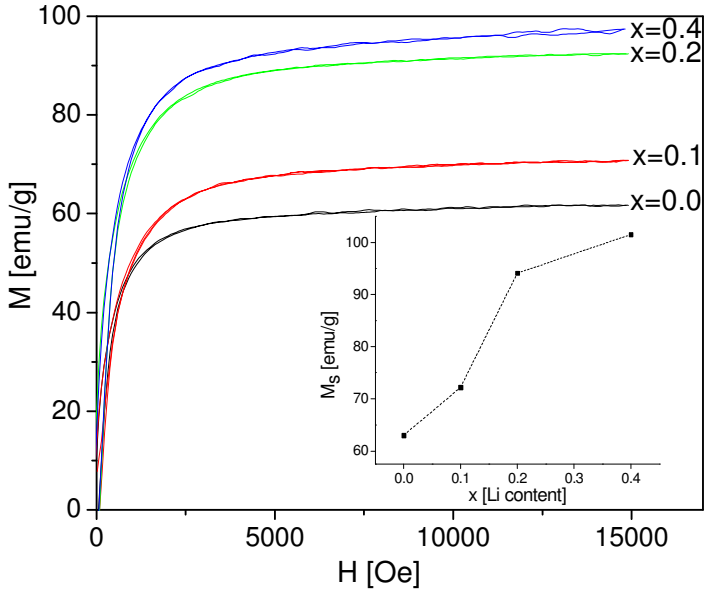

Figure 2: First quadrant of the hysteresis loops for all the samples as a function of Li content, x. The inset shows the increasing of saturation magnetization with x, before correction for secondary phases.

It is well-known that the magnetic properties of spinel ferrites depend on the vectorial sum of the magnetic moments at tetrahedral (A) and octahedral (B) sites which align anti-parallel to each other [24]. It has also been experimentally verified in numerous studies (see, for instance refs. [22] and [24]) that the distribution of cations among the lattice sites is strongly dependent on the material preparation. Therefore, an accurate determination of the cationic distribution in the lattice is important to account for the magnetic properties of the material.

Since different site occupation is translated into different relative intensities in the diffraction patterns, profile fitting by Rietveld analysis is one of the most used methods to determine cation distributions. Hence, for the correct assessment of the cationic distribution, an adequate magnetic structure model is required.

As different configurations may be effective in minimizing the quadratic differences between the observed and calculated spectra, the Rietveld method requires the use of a model for cationic distribution as close to the real one as possible so that the starting point for the refinement is not far from the converging values. The particular cation distribution or configuration which gives the best fit to the experimental diffraction patterns should also be appropriate for describing the increase in saturation magnetization M_S with Li content, x. Since magnetization in a ferrimagnetic compound is calculated as the difference between the magnetic moment in octahedral and tetrahedral sites, the increase in M can be achieved by either increment of B moments, decrease of A moments, or both.

For proposing an appropriate cationic model, different aspects had to be considered:

1. The system should be electrically neutral, that is –the sum of the ionic charges of cations in A and B sites should be equal to 8, in order to neutralize the charge corresponding to the four O^{2-} per unit formula.
2. The total magnetization should increase with x.
3. An inversion factor δ ($0<\delta<1$) had to be defined for each x value in order to consider the cationic distribution of 0.5x Li, (0.6 - x) Zn, 0.4 Mn, and (2+0.5x) Fe per unit formula.
4. Since the cations in sample 800 (x=0.0) are different from the ones with x≠0.0, different models were proposed to consider this fact.

After several attempts, in which all the above considerations had to be fulfilled, the following models were the best for fitting both structural and magnetic data:

- For sample 800 (x=0) model $\mathbf{M_0}$:
  $\left(Zn^{2+}_{0.6-\delta}Mn^{2+}_{0.4}Fe^{3+}_{\delta}\right)_A\left[Zn^{2+}_{\delta}Fe^{3+}_{2-\delta}\right]_B O^{2-}_4$

- For samples with x≠0 model $\mathbf{M_x}$:
  $\left(Li^{+}_{0.5x-\delta}Zn^{2+}_{0.4-0.5x-\delta}Mn^{2+}_{0.2-2\delta}Mn^{3+}_{0.2+2\delta}Fe^{2+}_{0.2+2\delta}\right)_A\left[Li^{+}_{\delta}Zn^{2+}_{0.2-0.5x+\delta}Fe^{3+}_{1.8+0.5x-2\delta}\right]_B O^{2-}_4$

Using these models for the refinements, it was found that Mn ions prefer tetrahedral coordination even when allowing some octahedral occupation, as the system converged to a B site occupation of zero for this cation. Only divalent Mn is appropriate for x=0.0 and for samples with Li both di- and trivalent states of Mn were considered. Therefore, a divalent state of Fe had to be also considered, in order to account for the natural balance $Fe^{3+} + Mn^{2+} \leftrightarrow Fe^{2+} + Mn^{3+}$ [25]. The possibility of a tetravalent state for Mn ion was disregarded on the basis of previous studies by Wende et al [7]. In addition, it is widely accepted that in mixed ferrites Zn ions occupy A sites. However, in this case, it was necessary to allow B sites occupation by Zn^{2+}, which is quite remarkable.

3.1. Rietveld refinement data

Figure 3a shows the Rietveld fit of sample 801 and Figure 3b displays the corresponding to sample 804. The refinements corresponding to the other samples are very similar and are not shown. Tables II-IV contain all the parameters and results obtained from the refinements.

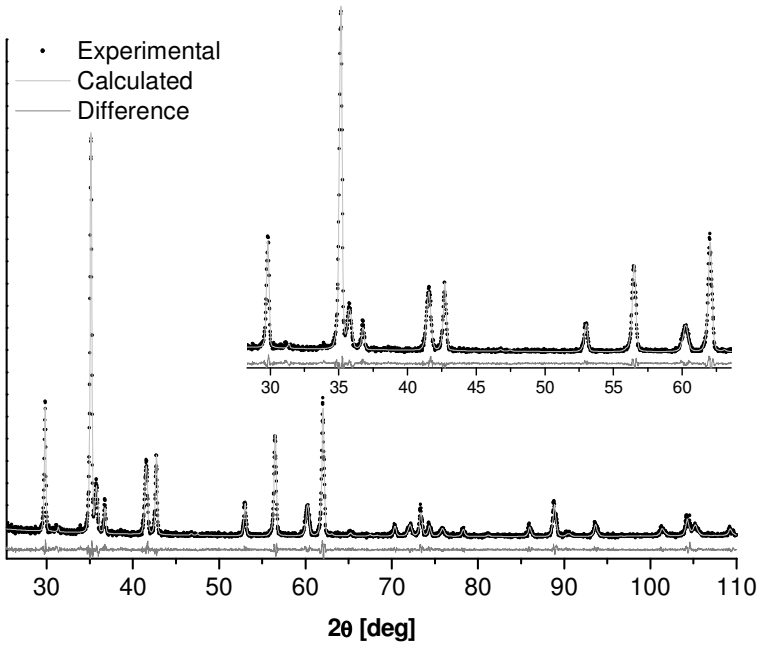

Figure 3a

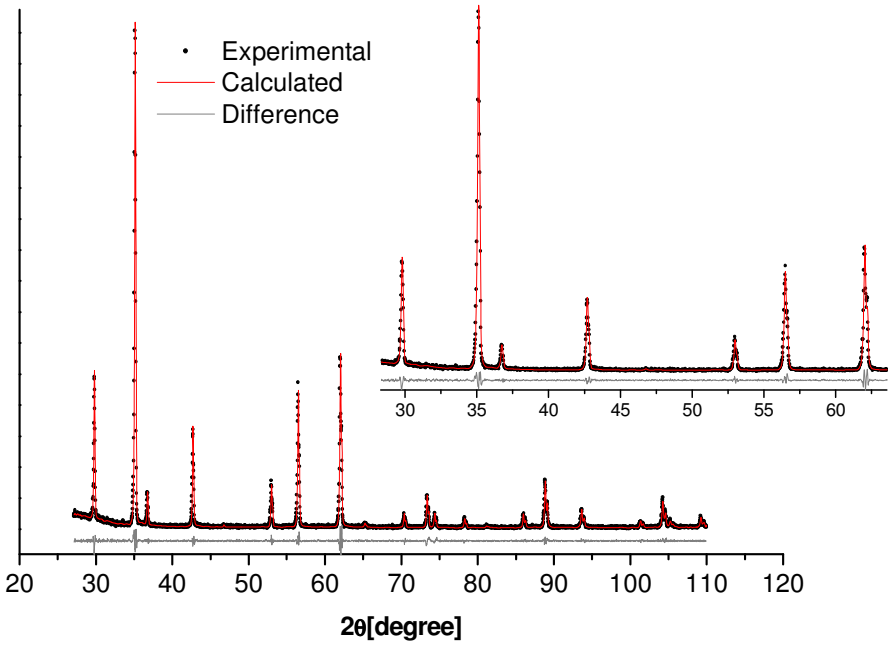

Figure 3b

Figure 3: Rietveld refinement of samples 801 (a, grey online) and 804 (b, red online). The inset is an enlargement of the portion with the most intense peaks. Circles indicate the observed intensity while the calculated pattern is shown as a solid curve. Below each spectrum, the difference between observed and calculated intensities can be seen.

Table II: Rietveld parameters indicating the quality of the refinements and different phase-content for all samples.

x	R_{exp} [%]	R_{wp} [%]	GoF	Ferrite [%]	FeO [%]	ZnO [%]
0.0	2.93	4.86	1.66	88.7±0.6	10.5 ±0.2	0.4 ± 0.1
0.1	3.20	4.66	1.46	79.0±0.5	20.6 ± 0.2	0.4 ± 0.1
0.2	2.53	3.79	1.50	93.8±0.8	6.2 ± 0.5	0.00± 0.01
0.4	2.20	3.07	1.40	100.00± 0.01	0.00± 0.01	0.00± 0.01

Table III: Cationic distribution in sites A and B for all samples. The uncertainties associated with the cationic occupation affect the last significant digit.

	Li^{+}		Zn^{2+}		Mn^{2+}		Mn^{3+}		Fe^{3+}		Fe^{2+}	
x	A	B	A	B	A	B	A	B	A	B	A	B
0.0	0.000	0.000	0.273	0.327	0.400	0.000	0.000	0.000	0.327	1.673	0.000	0.000
0.1	0.035	0.015	0.335	0.165	0.170	0.000	0.230	0.000	0.000	1.820	0.230	0.000
0.2	0.085	0.015	0.285	0.115	0.170	0.000	0.230	0.000	0.000	1.870	0.230	0.000
0.4	0.185	0.015	0.185	0.015	0.170	0.000	0.230	0.000	0.000	1.970	0.230	0.000

Table IV: Cell parameter, cell volume, cristal size and strain for all samples

x	a [±0.0001Å]	V [±1$Å^3$]	D [±0.2nm]	Strain ε_0 [±0.001]
0.0	8.4556	605	57.5	0.029
0.1	8.4902	612	55.4	0.033
0.2	8.4608	606	60.6	0.042
0.4	8.4409	601	84.2	0.059

The calculated strain values ε_0 (Table IV) increase with Li content. This provides further evidence that Li ions enter the spinel lattice. It is also noticed that the crystal size *D* in samples with lithium increases when the amount of secondary phases decreases, since minority phases usually tend to prevent grain growth.

The values of R_{wp} are higher for the samples with more secondary phases, but remained less than 5% in all the cases.

3.2 Mössbauer spectra

As it is widely accepted, Mn, Zn, and Fe cations in the spinel structure of MnZn ferrites are distributed among the two interstitial tetrahedral (A) and octahedral (B) sites. In general, Mössbauer spectra of MnZn ferrites may be fitted with one sextet corresponding to Fe in the A sites and another sextet corresponding to Fe in the B sites.

In this work, all the studied samples were fitted with two sextets {A} and {B} (one for each crystallographic site A and B) and a doublet {D1} to take into account the probable existence of small particles with low crystallinity.

Mössbauer spectra for x= 0.0, 0.1 and 0.2 were fitted with an additional doublet {D2} corresponding to the secondary phase (FeO) detected by XRD in those samples (Fig. 1 and Table 2).

Figures 4a and 4b show the room temperature spectra of samples 800 and 804, respectively. The corresponding fitting parameters are presented in Table V.

The six-line spectra for the samples were analyzed in terms of two sub-spectra. For x= 0.4, the sharper pattern can be due to Fe^{3+} ions at B–sites while the broader pattern may be due to Fe^{3+} and Fe^{2+} ions at A sites, as the IS value suggests (Table V). This result is in agreement with the proposed model for cation distribution (Section 3). The broadening of the A-pattern {A}, is interpreted as being due to the distribution of hyperfine fields at A sites, mainly caused by a random distribution of the cations at B sites [26].

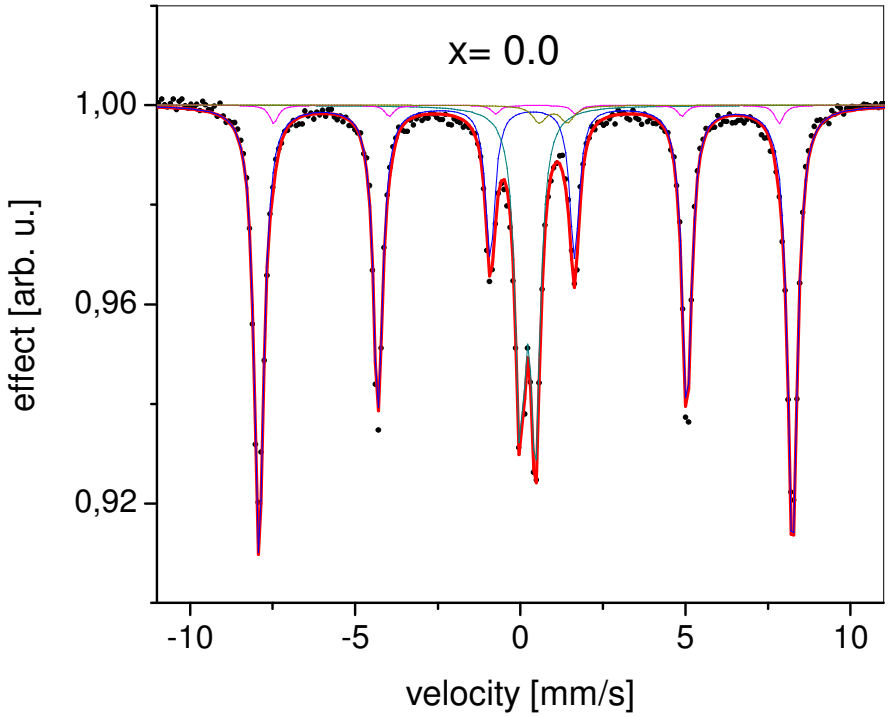

Figure 4a

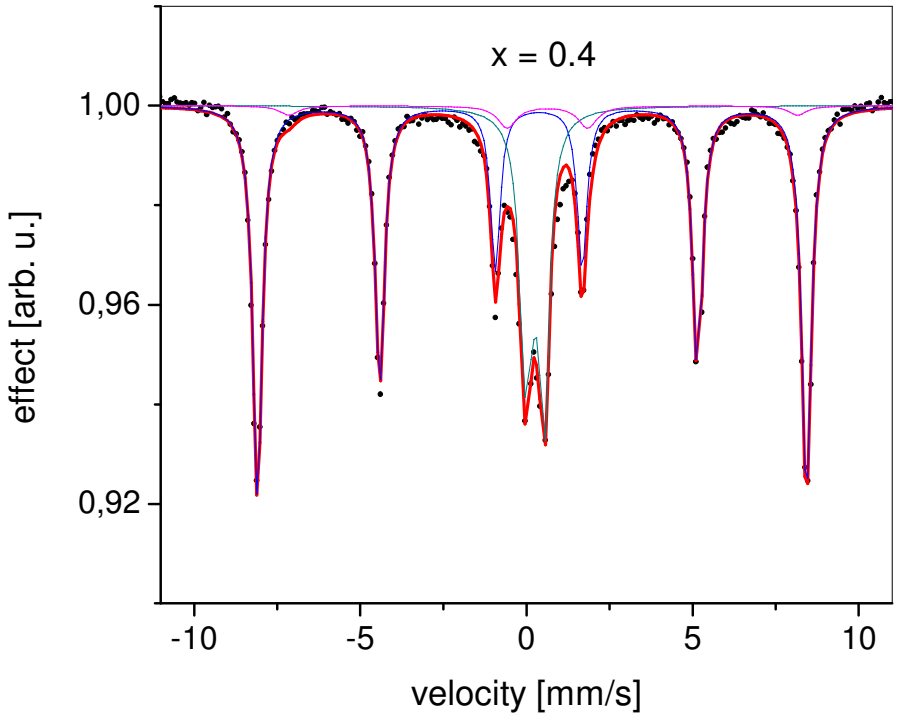

Figure 4b

Figure 4: Mössbauer spectra of samples 800 (a) and 804 (b).

Table V: Parameters derived from the Mössbauer analysis for sextets {A} and {B} and doublets {D1} and {D2}: B_{hf} (hyperfine magnetic field in Tesla), IS (isomer shift referred to α-Fe at RT), linewidth Γ and SA (relative spectral area of each component).

	{B} Γ 0.32mm/s			{A} Γ 0.40mm/s			{D1} Γ 0.40mm/s		{D2} Γ 0.50mm/s	
x	B_{hf} [T] (0.1)	IS [mm/s] (0.02)	SA (%)	B_{hf} [T] (0.1)	IS [mm/s] (0.02)	SA (%)	IS [mm/s] (0.02)	SA (%)	IS [mm/s] (0.02)	SA (%)
0.0	50.0	0.37	60.0	47.4	0.42	13.0	0.44	22.0	1.00	5.0
0.4	50.8	0.38	70.0	49.0	0.75	10.0	0.34	20.0	-	-

The presence of {D2} is related to antiferromagnetic FeO, as a singlet of these characteristics can be assigned to this phase [27].

The presence of {D1} can be related to the fact that a fraction of Fe ions have few nearest neighbors with ordered spins [26]. This fact makes it difficult to quantify the iron ions distribution between A and B sites.

Although an exact iron distribution is difficult to achieve by Mössbauer analysis, the presence of Fe^{3+} in the octahedral sites and the presence of Fe^{2+} –without discarding some contribution of Fe^{3+}– in the tetrahedral sites for the substituted samples, are a good support to the proposed model

3.3 Magnetic data

For those samples which are not single phase, the amount of secondary phases has to be considered when calculating magnetization in units of emu/g. Supposing that –at room temperature– the magnetic moments of each lattice site are perfectly anti-parallel to one another, saturation magnetization could be calculated by subtracting the magnetic moments of sites B and A, just as would be done at T=0 K. Let ${}^0M_s^t$ and ${}^xM_s^t$ be the theoretical saturation magnetization calculated with cationic distribution models $\mathbf{M_0}$ and $\mathbf{M_x}$, respectively, ${}^xM_s^c$ the corresponding value with mass correction and α_x the ferrite content. According to this, it is found that ${}^0M_s^t = (8 - 10\delta)\mu_B$ for samples without Li and ${}^xM_s^t = (6.4 + 2.5x - 16\delta)\mu_B$ for those with x≠0.0. The values of the refined inversion factor, the calculated values for ${}^0M_s^t$ and ${}^xM_s^t$ and corrected experimental saturation magnetization ${}^xM_s^c$ are shown in Table VI for samples with different Li content.

Table VI: Inversion factor, theoretical saturation magnetization per unit formula and corrected experimental saturation magnetization for all samples.

x	δ	${}^0M_S^t$ [±0.01μ_B]	${}^xM_S^t$ [±0.01μ_B]	${}^xM_s^c$[±0.1emu/g]
0.0	0.327000	4.73	-	74.7
0.1	0.015000	-	6.41	91.4
0.2	0.015000	-	6.66	100.3
0.4	0.009375	-	7.25	101.5

The Field Cooling reduced magnetization $M(T)/M_0$ curve of sample 800 is shown in Figure 5. Similar results were obtained for all samples. Because magnetic moments are not perfectly aligned at room temperature, there is an error when calculating the theoretical magnetization as the difference between B and A moments. Magnetization is reduced in about 12% when going from T=4 K to T=300 K. This effect must be considered when comparing the magnetization calculated from the proposed cationic model with the experimental data.

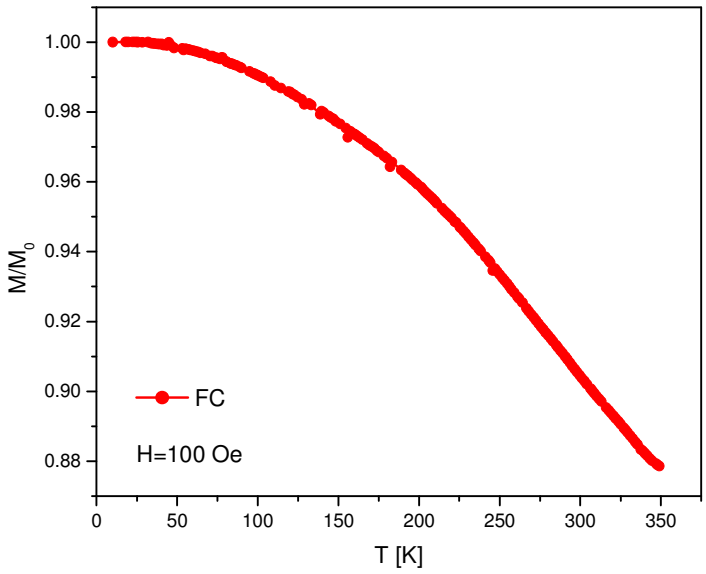

Figure 5: Field cooling M(T) curve for sample 800. The applied field is H=100 Oe.

A complete uncertainty analysis was performed for both calculated ($(M/M_0)_{Calc}$) and experimental ($(M/M_0)_{Exp}$) relative magnetizations. Besides the mentioned thermal effect for the error in calculated relative magnetization ($\Delta(M/M_0)_{Temperature}$), the error given by Rietveld refinement was also considered ($\Delta(M/M_0)_{Rietveld}$):

$$\Delta\left(\frac{M}{M_0}\right)_{Calc} = \Delta\left(\frac{M}{M_0}\right)_{Rietveld} + \Delta\left(\frac{M}{M_0}\right)_{Temperature}$$

The uncertainty in magnetization measurements is mainly influenced by mass measurements ($\Delta(M/M_0)_{Mass}$):

$$\Delta\left(\frac{M}{M_0}\right)_{Exp} = \Delta\left(\frac{M}{M_0}\right)_{Mass}$$

Comparison between experimental and theoretical relative magnetizations is shown in Table VII and Figure 6 along with their associated uncertainties.

Table VII. Comparison between experimental and theoretical relative magnetizations. The uncertainties are also shown.

x	$(M/M_0)_{Exp}$	$\Delta(M/M_0)_{Exp}$	$(M/M_0)_{Calc}$	$\Delta(M/M_0)_{Calc}$
0.0	1.00	0.07	1.00	0.05
0.1	1.22	0.08	1.36	0.05
0.2	1.34	0.09	1.41	0.05
0.4	1.36	0.09	1.5	0.1

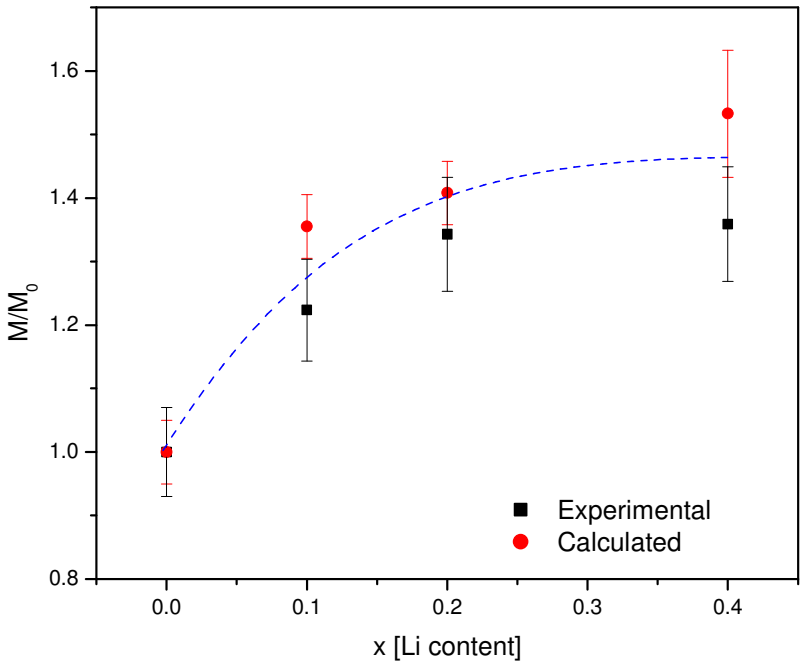

Figure 6: Comparison between relative $^{x}M_s^{c}$ (circles) and $^{x}M_s^{t}$ (squares). The dashed line is a guide for the eye.

Experimental and calculated values for saturation magnetization are indistinguishable within the error and follow the same behavior increasing with Li content, supporting the validity of the proposed cationic models.

Under the experimental conditions described for the studied samples, there is some Li and Zn preference towards A sites, which increases with Li substitution. The appearance of Mn^{2+} ions in octahedral sites is also observed with increasing x. Since the total magnetization is the difference M_B - M_A, the increase in Li and Zn A-occupancy together with the appearance of Mn^{2+} in octahedral sites (with a larger magnetic moment than Mn^{3+}) increases the net magnetization. Calculation of δ with Mössbauer parameters of iron occupancy in A and B sites (Table V) yields similar results ($\delta_{x=0} = 0.36$ and $\delta_{x=0.4} = 0.04$) to those obtained with Rietveld refinement (Table VI).

4. Conclusions

For the selected experimental conditions, substituting Li for Zn in Mn-Zn ferrite favorably contributes to a decrease of secondary phases and an increase in saturation magnetization. The magnetic and structural observed properties were explained by introducing an adequate cationic distribution model, which considers both tetrahedral as well as octahedral sites for Zn ions.

The presence of the doublet D1 in the Mössbauer RT spectra makes it difficult to quantify iron ions distribution between A and B sites. However, the existence of the six–line magnetic pattern due to the superexchange interaction between the magnetic ions at tetrahedral (A) and octahedral (B) sublattices and the raise in the hyperfine fields (B_{hf}) of A and B sites suggest an enhancement in magnetic coupling, which is evidenced in the increase of Ms.

Lithium substitution favors ion migration to the different crystalline sites. This is supported by the obtention of a single phase material and no segregated phases for x>0.3.

Acknowledgements
This work was partially funded by Secyt-UNC and Conicet. M. Arana acknowledges a doctoral fellowship from Conicet and V. Galván acknowledges a post-doctoral position from Conicet.

References
1. P. Hu, H. Yang, D. Pan, H. Wang, J. Tian, S. Zhang, X. Wang, A. A. Volinsky, J. Magn. Magn. Mater., 322 (2010) 173-177.
2. L. Nèel, Science 3 (1971) 985- 92, DOI:10.1126/science.174.4013.985.
3. Y. M. Abbas, S. A. Mansour, M. H. Ibrahim, E. Shehab, J. Magn. Magn. Mater., 323 (2011) 2748-2756.
4. J. Li, H. Yuan, G. Li, Y. Liu, J. Leng, J. Magn. Magn. Mater. (2010), doi:10.1016/j.jmmm.2010.06.035.
5. C. M. B. Henderson, J. M. Charnock, D. A. Plant, J. Phys. Condens. Matter, 19 (2007) 076214 25 doi:10.1088/0953-8984/19/7/076214.
6. S. Bid, S. K. Pradhan, Mat. Chem. Phys., 84 (2004) 291-301.
7. C. Wende, K. Olimov, H. Modrow, F. E. Wagner, H. Langbein, Mat. Res. Bull, 41 (2006) 1530-1542.
8. S. Bid, P. Sahu, S. K. Pradhan, Phys. E, 39 (2007) 175-184.
9. S. Bid, S. K. Pradhan, Mat. Chem. Phys., 82 (2003) 27-37.
10. H. Demidzu, T. Nakamura, Y. Yamada, J. of Magn. Magn. Mater., 322 (2010) 1816-1821.
11. P. P. Hankare, R. P. Patil, U. B. Sankpal, S. D. Jadhav, I. S. Mulla, K. M. Jadhav, B. K. Chougule, J. Magn. Magn. Mater., 321 (2009) 3270–3273
12. T. Abbas, Y. Khan, M. Ahmad, S. Anwar, Sol. St. Comm, 82(9) (1992) 701-703.
13. B. Guillot, M. E. Guendouzi, J. Sol. St. Chem., 106 (1993) 403-450.
14. C. Venkataraju, G. Sathishkumar, K. Sivakumar, J. Magn. Magn. Mater., 322 (2010) 230-233.
15. M. Javad, N. Isfahani, M. Myndyk, D. Menzel, A. Feldhoff, J. Amighian, V. Šepelàk, J. Magn. Magn. Mater., 321 (2009) 152-156.
16. P. Singh, A. Sil, M. Nath, S. Ray, Phys. B, 405 (2010) 649-654.
17. J. Lai, K. V. P. M. Shafi, A. Ulman, N. Yang, M. Cui, T. Vogt, C. Estounès, Am. Chem. Soc., Div. Fuel Chem., 48(2) (2003) 729-730.
18. V. Chlan, P. Novák, J. Magn. Magn. Mater., 322 (2010) 1056-1058.
19. E. De Fazio, P. G. Bercoff, S. E. Jacobo, Solid State Phenomena 168 – 169 (2011) 353-356.
20. E. De Fazio, P. G. Bercoff, S. E. Jacobo, J. Magn. Magn. Mater., 323 (2011) 2813-2817.
21. R. Young, The Rietveld Method, International Union of Crystallography, Oxford University Press, Oxford, 1993
22. D. Balzar, Voigt-function model in diffraction line-broadening analysis. Microstructure Analysis from Diffraction, R. L. Snyder, H. J. Bunge, and J. Fiala, International Union of Crystallography, 1999
23. L. B. McCusker, R. B. Von Dreele, D. E. Cox, D. Louer, P. Scardi, Journal of Applied Crystallography,32 (1999) 36-50.
24. J. Smit, H. P. J. Wijn, Ferrites, physical properties of ferrimagnetic oxides in relation to their technical applications, N. V. Philip's Gloeilampenfabrieken, Eindhoven, 1959
25. Q. Wei, J. Li, Y. Chen, Y. Han, Materials Chemistry and Physics, 74 (2002) 340–343.
26. D. C. Dobson, J. W. Linnet, M. M. Rahman, *J. Phys. Chem. Solids* 31, 727 (1970).
27. T. Yoshikawa, Y. Kanke, H. Yanagihara, E. Kita,·Y. Tsunoda, K. Siratori, K. Kohn, *Hyperfine Interact.* DOI 10.1007/s10751-011-0550.